Seasonal and diurnal variations of submicron organic aerosol in Tokyo observed using the Aerodyne aerosol mass spectrometer

N. Takegawa,[1] T. Miyakawa,[1] Y. Kondo,[1] J. L. Jimenez,[2] Q. Zhang,[3] D. R. Worsnop,[4] and M. Fukuda[1]

Received 19 July 2005; revised 14 January 2006; accepted 3 March 2006; published 7 June 2006.

[1] In situ measurements of trace gases and aerosols were conducted at an urban site in Tokyo (35°39′N, 139°40′E). The data obtained in summer (July–August 2003), fall (September–October 2003), and winter (February 2003 and January–February 2004) are used for the present analysis. Size-resolved chemical composition of nonrefractory (vaporized at 600°C under high vacuum) submicron aerosol was measured using an Aerodyne aerosol mass spectrometer (AMS). Organics are found to be the dominant component (40–60% of total nonrefractory aerosol mass) in all periods. Organic aerosol (OA) is classified by correlation with carbon monoxide (CO) and fragments of aliphatic and oxygenated organic compounds in the AMS mass spectra. Combustion-related organic aerosol (combustion OA) is defined as the primary organic aerosol (POA) fraction, as determined by a linear correlation with CO. Excess organic aerosol (excess OA) is defined by subtracting the combustion OA and the background OA from the total OA. The combustion OA and excess OA show good correlation (r^2 = 0.65–0.85) with hydrocarbon-like organic aerosol (HOA) and oxygenated organic aerosol (OOA), respectively, which were derived from a custom principal component analysis. In the summer period the estimated excess OA concentrations show distinct diurnal variations and correlate with ozone (O_3) during daytime. On average, the combustion OA does not exhibit a distinct diurnal variation for the summer, fall, and winter periods, while the excess OA shows a clear diurnal pattern (daytime peak at ~1300 LT). At the daytime peak the excess OA is found to be at nearly the same concentration as the combustion OA for all seasons, suggesting that significant formation of secondary organic aerosol (SOA) occurred in daytime throughout the measurement period.

Citation: Takegawa, N., T. Miyakawa, Y. Kondo, J. L. Jimenez, Q. Zhang, D. R. Worsnop, and M. Fukuda (2006), Seasonal and diurnal variations of submicron organic aerosol in Tokyo observed using the Aerodyne aerosol mass spectrometer, *J. Geophys. Res.*, *111*, D11206, doi:10.1029/2005JD006515.

1. Introduction

[2] Urban areas are large sources of anthropogenic gaseous species and particulate matter. High concentrations of aerosols in urban air have adverse effects on human health [e.g., *NARSTO*, 2004]. In addition to this local influence, export of anthropogenic aerosols from urban areas to surrounding regions can significantly affect the air quality and radiative balance in those regions as well. Previous studies have shown that organic compounds constitute a substantial fraction of total fine particle mass in urban air [e.g., *Chow et al.*, 1994; *Gray et al.*, 1986]. However, the chemical composition and formation mechanisms of organic aerosols are not fully understood because organic aerosols consist of hundreds to thousands of chemical species with a very wide range of chemical and thermodynamic properties [e.g., *Alves et al.*, 2002; *Saxena and Hildemann*, 1996; *Turpin et al.*, 2000].

[3] Emissions from motor vehicles (gasoline and diesel) can be important sources of primary organic aerosol (POA) in urban areas [*Rogge et al.*, 1993a]. It has been found that POA from vehicular exhaust is mainly composed of long-chain *n*-alkanes and branched cycloalkanes and includes a number of chemical species such as *n*-alkanoic acids, aldehydes, and polycyclic aromatic hydrocarbons (PAHs) [*Reilly et al.*, 1998; *Rogge et al.*, 1993a, 1993b; *Tobias et al.*, 2001]. Primary emissions of dicarboxylic acids were also identified in vehicular exhaust [*Kawamura and Kaplan*, 1987]. Secondary organic aerosol (SOA) is formed via oxidation of volatile organic compounds (VOCs) followed by condensation on existing particles or by homoge-

[1]Research Center for Advanced Science and Technology, University of Tokyo, Tokyo, Japan.
[2]Department of Chemistry and Biochemistry and Cooperative Institute for Research in Environmental Sciences, University of Colorado, Boulder, Colorado, USA.
[3]Atmospheric Science Research Center, University at Albany, State University of New York, Albany, New York, USA.
[4]Center for Aerosol and Cloud Chemistry, Aerodyne Research, Inc., Billerica, Massachusetts, USA.

0148-0227/06/2005JD006515$09.00

neous nucleation. Smog chamber experiments have shown that aromatic hydrocarbons (toluene, xylene, etc.) from gasoline vapor can be a significant source of SOA in urban air [*Odum et al.*, 1997]. Biogenic hydrocarbons also make a substantial contribution to the SOA in some urban areas [*Szidat et al.*, 2004]. Atmospheric measurements in urban areas have identified a large amount of water-soluble organic carbon (WSOC), which is likely the major constituent of SOA [*Saxena and Hildemann*, 1996; *Sullivan et al.*, 2004]. WSOC generally consists of oxygenated organic compounds containing various functional groups such as alcohols, carbonyls, and dicarboxylic acids [*Alves et al.*, 2002; *Kawamura and Ikushima*, 1993; *Saxena and Hildemann*, 1996].

[4] An assessment of the contributions of primary emissions and secondary formation to ambient organic aerosol loadings in urban areas is important for developing regulatory strategies for particulate matter (PM) control. It is also important for estimating direct/indirect forcing of organic aerosols because hygroscopic properties of organic aerosols depend upon the chemical composition [*Saxena et al.*, 1995]. In practice, unambiguous separation of POA and SOA in ambient air is generally difficult to achieve. Alternatively, classification of ambient organic aerosols according to certain criteria (e.g., chemical class and/or correlation with tracers) provides useful qualitative insights into the relative fractions and temporal profiles of POA and SOA.

[5] The Aerodyne aerosol mass spectrometer (AMS) can measure size-resolved chemical composition of ambient nonrefractory (vaporized at 600°C under high vacuum) submicron aerosol for an integration time of the order of minutes [*Jayne et al.*, 2000; *Jimenez et al.*, 2003a]. Mass spectra obtained with the AMS provide useful information with which to classify organic aerosol according to chemical classes. *Zhang et al.* [2005a] have developed a new method to separate hydrocarbon-like organic aerosol (HOA) and oxygenated organic aerosol (OOA) based on custom principal component analysis of the AMS mass spectra. This method offers the advantage of providing not only mass concentrations but also mass spectra of HOA and OOA.

[6] In this paper we use AMS data obtained in Tokyo to investigate the seasonal and diurnal variations of organic aerosol in this region. The observed organic aerosol (OA) is classified based on correlation with carbon monoxide (CO) and fragments of aliphatic and oxygenated organic compounds in the AMS mass spectra. The combustion-related organic aerosol (combustion OA) is defined as the POA fraction, as determined by a linear correlation with CO. The excess organic aerosol (excess OA) is defined by subtracting the combustion OA and the background level of OA from the total OA. The basis of this classification is similar to the elemental carbon (EC) tracer method proposed by *Turpin and Huntzicker* [1995]. If the emissions of POA and CO are dominated by combustion sources and the emission ratio of POA to CO can be regarded as nearly constant, the combustion OA and excess OA may be good approximations of POA and SOA, respectively. However, we use the former terminology for the present analysis to make the definition clear. The major purpose of this paper is to investigate the seasonal and diurnal variations of the combustion OA and excess OA in Tokyo during the measurement period.

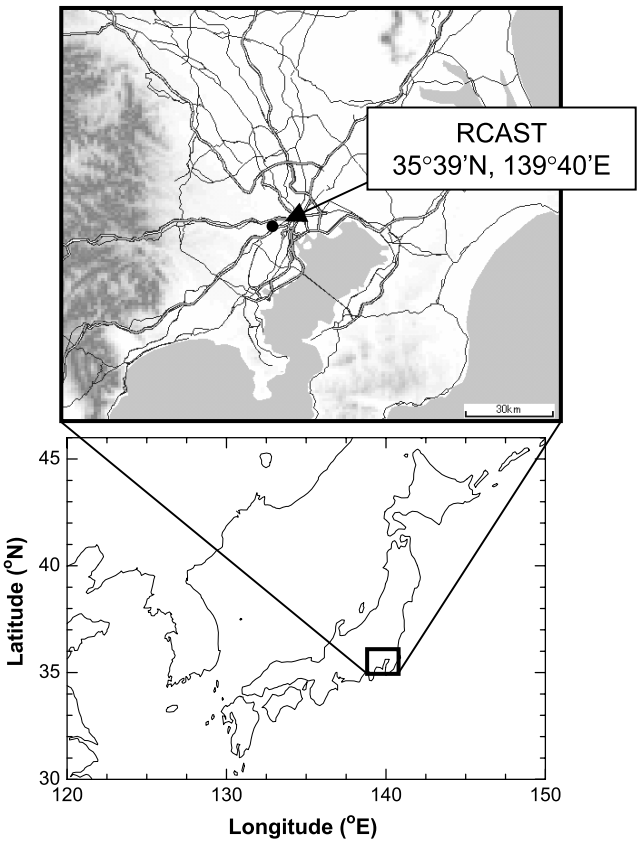

Figure 1. Map of the Tokyo metropolitan area and location of the Research Center for Advanced Science and Technology (RCAST) observatory. In the top panel, bold lines represent heavy-traffic highways and thin lines represent major roads.

2. Ground-Based Measurements in Tokyo

2.1. Instruments

[7] In situ measurements of trace gases and aerosols have been conducted at a surface site in Tokyo. The population of the southern Kanto area, including Tokyo and three surrounding prefectures, is ~33 million at present. The data obtained in February 2003 (winter1 period), July–August 2003 (summer period), September–October 2003 (fall period), and January–February 2004 (winter2 period) are used in this study. The winter1 and winter2 periods are combined (referred to simply as winter period) unless we specifically describe the difference between the winter1 and winter2 periods. This series of intensive measurement periods is referred to as the Integrated Measurement Program for Aerosol and oxidant Chemistry in Tokyo (IMPACT). The IMPACT campaign is the first systematic study focusing on megacities in East Asia. Figure 1 shows a map of the Tokyo area. The observation site is on the top (fifth) floor of a building on the campus of the Research Center for Advanced Science and Technology (RCAST), University of Tokyo (35°39′N, 139°40′E). RCAST is located near the center of the city and surrounded by heavy traffic highways

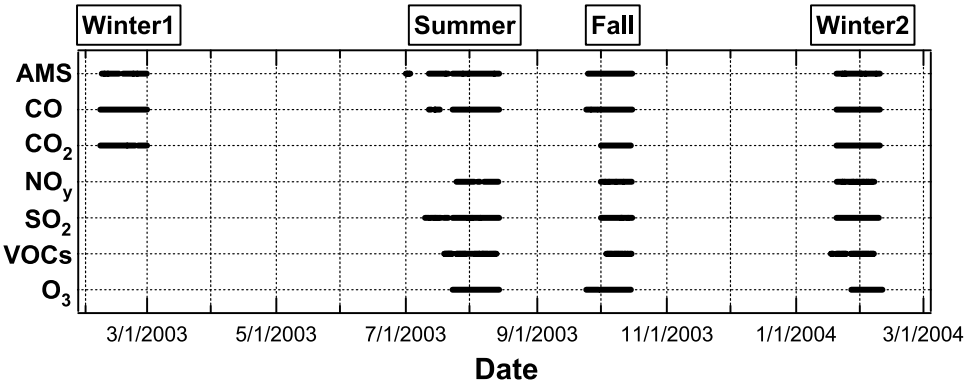

Figure 2. Time periods with measurements of chemical species that are mainly used in this analysis.

(at about ~2 km distance from the observatory). The sample air was aspirated from the rooftop of the observatory building (~18 m above ground level and ~57 m above mean sea level). Figure 2 summarizes the data coverage of the chemical species that are mainly used in this analysis. Although ambient measurements were also performed in April–June 2003, these data are not used in this analysis because the number of data samples is limited.

[8] Size-resolved chemical composition of nonrefractory submicron aerosol, which is hereafter referred to as NR-PM_1, was measured using an AMS. Details of the performance of our AMS including the stability of the instrument sensitivity and intercomparison with other aerosol measurements are presented by *Takegawa et al.* [2005]. In this paper the mass concentrations of aerosol measured by the AMS are reported in units of $\mu g\ m^{-3}$ at 20°C and 1 atm (10 min averages). The date and time are reported in Japanese local time (UTC + 09:00).

[9] CO was measured using a nondispersive infrared absorption (NDIR) instrument with an integration time of 1 min (Model 48, Thermo Environmental Instruments (TEI), USA.). In order to reduce the interference from water vapor (H_2O), the sample air for the CO instrument was dried (dew point <0°C) using a Nafion dryer (Perma-Pure, Inc., USA.). The background (zero) signals were routinely measured every 1 or 2 hours by supplying purified (dry) air into the sample line. The zero signals measured using the purified air agreed well with those measured using a Hopcalite scrubber (CO removal catalyst) after passing the sample air through the Nafion dryer. The uncertainty in determining the zero signals was estimated to be ~15 parts per billion by volume (ppbv) (1σ). Calibrations were performed at the beginning of each measurement period by supplying a CO standard (5 parts per million by volume (ppmv) CO in air) manufactured by the Nissan-Tanaka Corp., Japan. The stability of the instrument sensitivity (i.e., stability of the calibration signals) was ~1.5% (1σ) between February 2003 and February 2004. The overall precision and accuracy of the 1 min CO data were estimated to be 4 ppbv and 20 ppbv, respectively, at a CO mixing ratio of 400 ppbv.

[10] Carbon dioxide (CO_2) was measured using an NDIR-based instrument with an integration time of 10 s (Model LI7000, Li-Cor, Inc., USA). The sample line for the CO_2 instrument was the same as that for the CO instrument so as to reduce the interference from H_2O. The offset level of the NDIR signal was automatically corrected by the internal zero system (i.e., CO_2 removal catalyst). In addition to this, external calibrations were performed at the beginning and end of each measurement period. The CO_2 standards used for the calibrations were 348 ppmv CO_2 in air (low standard) and 694 ppmv CO_2 in air (high standard) (Nissan-Tanaka Corp., Japan). The CO_2 offset level was determined using the low standard, and the instrument sensitivity (i.e., NDIR signal per ppmv CO_2) was determined using the difference between the high and low standards. The uncertainty in determining the offset level was estimated to be 1.5 ppmv (1σ) and the stability of the instrument sensitivity was ~1% (1σ). The precision and accuracy of the 10 s CO_2 data were estimated to be 0.3 ppmv and 2 ppmv, respectively, at a CO_2 mixing ratio of 400 ppmv. The meteorological parameters (ambient temperature, relative humidity, etc.) were measured using a standard meteorological station (Vaisala, Helsinki, Finland) with an integration time of 10 min.

[11] Ozone (O_3) was measured using an ultraviolet (UV) absorption instrument with an integration time of 1 min (Model 1101, Dylec, Japan). The Model 1101 was compared with another UV absorption O_3 instrument (Model 43, TEI, USA). These two measurements agreed well to within 4%. Nitrogen oxides (NO_x = NO + NO_2) and total reactive nitrogen (NO_y) were measured using a NO-O_3 chemiluminescence detector combined with a photolytic converter and a gold tube catalytic converter. The NO and NO_y instrument used in this study was originally designed for aircraft measurements [*Kondo et al.*, 1997] and was slightly modified for ground-based measurements. NO_y compounds were catalytically converted to NO on the surface of a gold tube heated at 300°C. The photolytic converter system used for the NO_2 measurement was manufactured by Droplet Measurement Technologies, Inc., USA. SO_2 was measured using a pulsed fluorescence technique with an integration time of 1 min (Model 43C, TEI, USA). Online VOC measurements (C_2–C_7 alkanes, alkenes, alkynes, and aromatics) were conducted using a GC-FID system combined with a preconcentration unit [*Enomoto et al.*, 2005]. The system is capable of measuring VOCs with a time resolution of 1 hour.

2.2. General Characteristics of Observed Air Masses

[12] First, the spatial representativeness of the observed air masses is examined. Figure 3 shows time series of CO

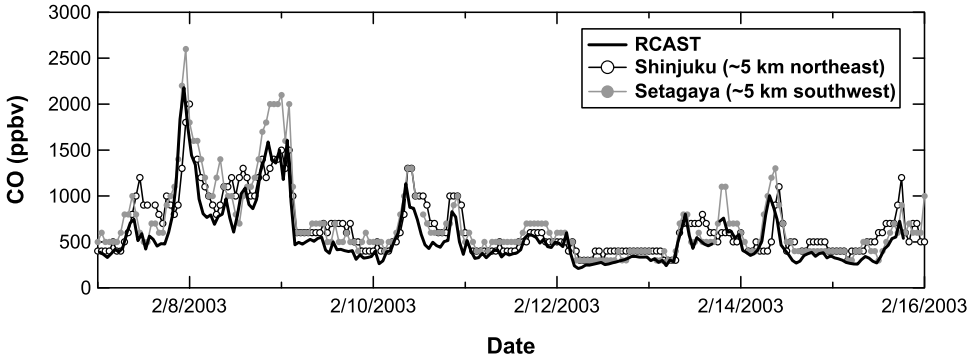

Figure 3. Time series of CO mixing ratios in February 2003 measured at the RCAST observatory (solid line), the Shinjuku monitoring station (open circles and line), and the Setagaya monitoring station (shaded circles and line).

mixing ratios measured at the RCAST observatory and two routine monitoring stations maintained by the Tokyo Metropolitan Government. The Shinjuku monitoring station is located in the center of the city (~5 km northeast of RCAST), and the Setagaya station is located in a residential area (~5 km southwest of RCAST). The three measurements show similar temporal variations, indicating that the air masses observed at RCAST were not significantly affected by a particular local source.

[13] Second, air flow patterns around the RCAST observatory are described. In the summer period, large-scale air flow patterns over Japan were determined by the North Pacific anticyclone, and maritime air was generally transported from the south. In addition, sea-land breeze circulation took place when a stable anticyclone was located over the Tokyo area. In the fall period, wind directions were mostly northerly, although weather conditions frequently changed associated with the passage of cyclones. In the winter period, air flow patterns in the Tokyo area were strongly influenced by northerly winds from the Siberian High. The CO mixing ratios tend to be higher with lower wind speed (and vice versa). The relationship between CO and wind speed did not show significant dependence on wind direction. This result suggests that wind speed (i.e., dilution rate) was one of the major controlling factors affecting the levels of CO mixing ratios and also suggests an absence of large point sources of CO around the RCAST observatory.

[14] Third, possible emission sources affecting the observed air masses are examined. According to an emission inventory for the Kanto area with a 10 km × 10 km resolution [*Kannari et al.*, 2004], emissions from vehicular sources (both diesel and gasoline) can account for ~80% of the CO emissions sources in the regions surrounding the RCAST observatory (approximately 60 km × 70 km area). Here we use the correlation of CO versus CO_2 to investigate the validity of this estimate. Figure 4 shows a scatter plot of CO versus CO_2 observed in the fall and winter periods, where every point represents a 10 min average. Note that CO_2 data were not obtained in the summer period. The $\Delta CO/\Delta CO_2$ ratio, defined as the linear regression slope, reflects the combustion efficiency of the emission sources [*Takegawa et al.*, 2004]. The $\Delta CO/\Delta CO_2$ ratio was 11.6 ppbv $ppmv^{-1}$ for the fall period and 10.7 ppbv $ppmv^{-1}$ for the winter period. On the other hand, the average CO/CO_2 emission ratio from vehicular sources is calculated to be ~17 ppbv $ppmv^{-1}$ based on the emission inventory. The other significant CO emission sources in Tokyo (industry

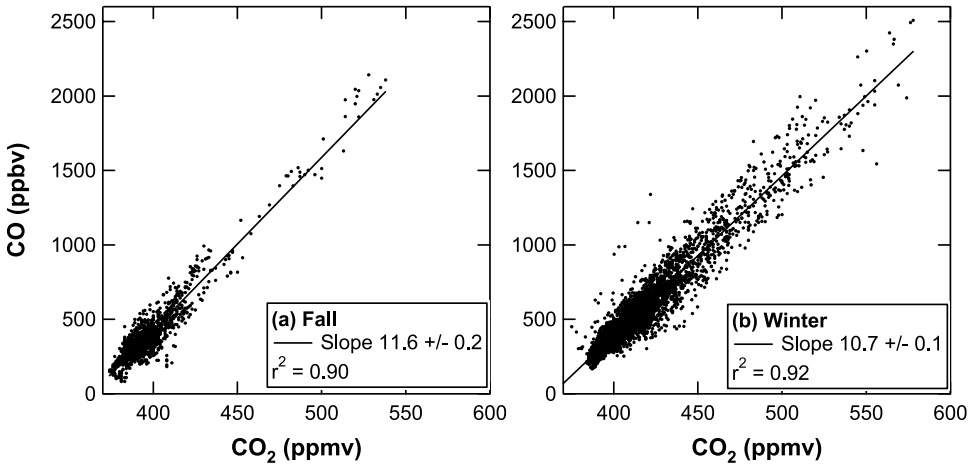

Figure 4. Scatterplots of CO versus CO_2 in the (a) fall and (b) winter periods. The solid line is the linear regression line.

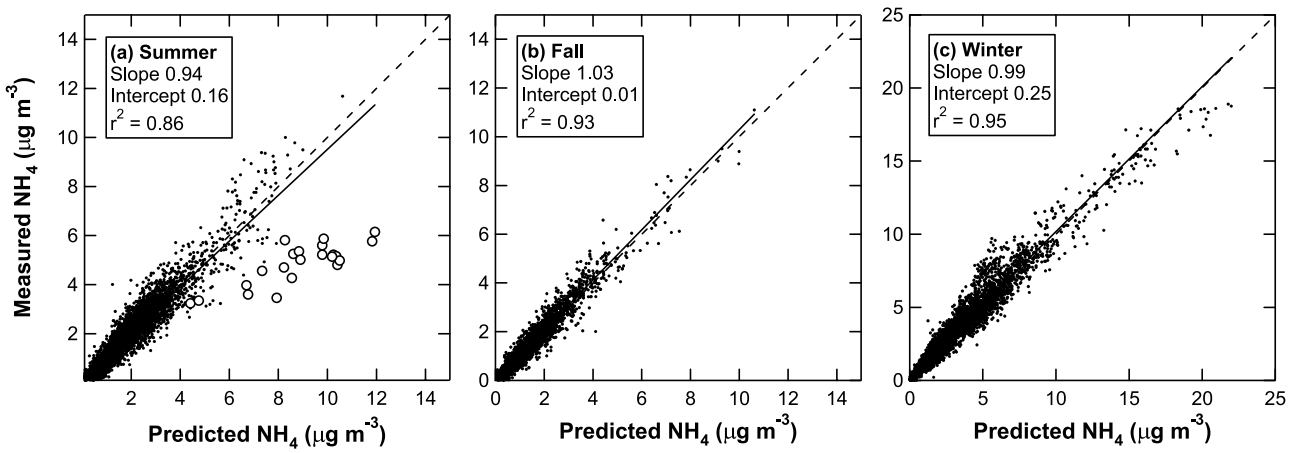

Figure 5. Scatterplot of measured and predicted ammonium (NH_4^+) for the (a) summer, (b) fall, and (c) winter periods. The solid line is the linear regression line, and the dashed line represents the 1:1 correspondence line. The predicted NH_4^+ was determined assuming that nitrate (NO_3^-), sulfate (SO_4^{2-}), and chloride (Cl^-) were fully neutralized by NH_4^+. The open circles indicate acidic particles.

and power plants) show much smaller CO/CO_2 emission ratios (3.8 ppbv $ppmv^{-1}$ and 0.1 ppbv $ppmv^{-1}$, respectively). The observed $\Delta CO/\Delta CO_2$ ratios were closer to the CO/CO_2 emission ratios from vehicular sources than those from industry and power plants in Tokyo. It is important to note that CO and CO_2 exhibited tight correlations (r^2 = 0.91–0.92) without significant seasonal variations, indicating that the types of CO emission sources surrounding the RCAST observatory did not have a large variability during the measurement period.

3. Results and Discussion

3.1. Mass Loadings

[15] Figure 5 depicts a scatter plot of measured and predicted ammonium (NH_4^+) for the summer, fall, and winter periods. The predicted NH_4^+ ($\mu g\ m^{-3}$) was determined assuming that nitrate (NO_3^-), sulfate (SO_4^{2-}), and chloride (Cl^-) were fully neutralized by NH_4^+:

$$\text{Predicted } NH_4^+ = MW_{NH4}\left(m(NO_3^-) + 2m(SO_4^{2-}) + m(Cl^-)\right), \quad (1)$$

where m(X) is the molar concentration of species X expressed in $\mu mol\ m^{-3}$ (at 20°C and 1 atm) and MW_{NH4} is the molecular weight of NH_4^+. In the summer period, there were some outlying data points indicative of acidic particles. These events were found under southerly or southwesterly conditions (wind direction 180°–250°) with very high SO_2 mixing ratios (10–35 ppbv). It is likely that these air masses were strongly influenced by SO_2 emissions from the Miyake Island volcano (34°04′N, 139°30′E), which is located ~180 km south from RCAST (T. Miyakawa et al., manuscript in preparation, 2006). For details about the Miyake Iisland volcano, the reader is referred to *Kajino et al.* [2005]. The number of these outlying data points was less than 1% of the total data points in the summer period. The regression slopes (including all data points) ranged from 0.94 to 1.03, indicating that nitrate, sulfate, and chloride detected by the AMS were mostly in the form of ammonium nitrate (NH_4NO_3), ammonium sulfate ($(NH_4)_2SO_4$), and ammonium chloride (NH_4Cl), respectively.

[16] Table 1 summarizes the median values of ambient temperature, mass concentration of NR-PM_1 aerosol, and mixing ratios of trace gases for each measurement period. Figure 6 shows mass concentrations of nitrate, sulfate, ammonium, and organics and their fractions of the total NR-PM_1 mass in the summer, fall, and winter periods. The 12 hour average data were used for the time series plots. As shown in Table 1, the median mass concentrations of total NR-PM_1 aerosol (= $NO_3^- + SO_4^{2-} + Cl^- + NH_4^+$ + organics) did not show significant seasonal variation during the measurement periods, ranging from 12 to 15 $\mu g\ m^{-3}$. Organics were found to be the dominant component throughout the measurement periods (5.7–7.1 $\mu g\ m^{-3}$, 40–60% of the total). The mass concentration and fraction of nitrate were higher in winter (2.8–3.1 $\mu g\ m^{-3}$, 20% of the total) than in summer (1.0 $\mu g\ m^{-3}$, 8% of the total), while those of sulfate were higher in summer (3.2 $\mu g\ m^{-3}$, 25%) than in winter (1.7–2.5 $\mu g\ m^{-3}$, 12–16%).

[17] The formation of $(NH_4)_2SO_4$ depends mainly on the production rate of sulfuric acid (H_2SO_4) and the concentration of ammonia (NH_3). The formation of NH_4NO_3 depends on the production rate of total nitrate ($HNO_3 + NO_3^-$), concentrations of NH_3 and sulfate, temperature, and relative humidity (RH). The thermodynamic equilibrium of NH_4NO_3 in Tokyo during the summer, fall, and winter2 periods has been investigated using the time-resolved observations of HNO_3, NH_3, and aerosol inorganic compounds [*Morino et al.*, 2006], *Morino et al.* [2006] have shown that the median mixing ratios of total ammonium ($NH_3 + NH_4^+$) were higher by a factor of 2–4 than those of the sum of sulfate and total nitrate during the summer, fall, and winter2 periods, indicating that the availability of NH_3 was not a major controlling factor determining the seasonal variations of nitrate and sulfate during the measurement period.

[18] In order to evaluate the production rates of nitrate and sulfate, hydroxyl radical (OH) concentrations were

Table 1. Summary of Ground-Based Measurements in Tokyo[a]

Parameters	Winter 1 (Feb 2003)	Summer (Jul–Aug 2003)	Fall (Sep–Oct 2003)	Winter 2 (Jan–Feb 2004)
Air temperature, °C	5.9 (4.0–8.3)	23.7 (21.2–26.1)	18.2 (16.4–20.9)	5.6 (3.6–7.9)
Nitrate, μg m^{-3}	3.1 (0.8–8.7)	1.0 (0.4–2.3)	1.0 (0.5–2.9)	2.8 (1.3–5.6)
Sulfate, μg m^{-3}	2.5 (1.5–3.6)	3.2 (2.0–4.7)	1.8 (1.1–2.6)	1.7 (1.2–2.5)
Chloride, μg m^{-3}	0.5 (0.2–1.1)	0.09 (0.03–0.2)	0.1 (0.05–0.3)	0.5 (0.2–1.1)
Ammonium, μg m^{-3}	2.2 (1.1–4.7)	1.8 (1.0–2.7)	1.3 (0.7–2.0)	2.3 (1.4–3.9)
Organics, μg m^{-3}	6.7 (3.4–10.5)	5.7 (3.5–8.9)	7.1 (4.6–10.3)	5.8 (3.7–9.4)
Total NR-PM_1, μg m^{-3}	15.3 (7.7–30.1)	12.7 (8.3–18.3)	11.9 (8.0–17.5)	14.0 (8.6–22.7)
CO, ppbv	435 (330–562)	358 (255–523)	328 (261–436)	489 (357–672)
CO_2, ppmv	405 (395–417)	N/A	394 (387–403)	409 (398–425)
C_6H_6, ppbv	N/A	0.30 (0.19–0.68)	0.36 (0.27–0.51)	0.62 (0.48–0.89)
C_7H_8, ppbv	N/A	1.58 (0.96–2.77)	2.46 (1.62–4.55)	3.17 (1.79–5.04)
NO_x, ppbv	N/A	14.0 (9.5–20.6)	23.7 (15.1–42.4)	38.4 (22.2–58.0)
NO_y, ppbv	N/A	26.7 (17.0–45.2)	28.6 (20.1–47.2)	41.2 (24.4–63.2)
SO_2, ppbv	N/A	1.36 (0.61–3.43)	0.78 (0.30–1.85)	1.82 (1.06–3.15)
O_3, ppbv (all data)	N/A	16.5 (5.8–29.6)	17.0 (6.5–30.0)	15.4 (3.8–28.4)
O_3, ppbv (1000–1600 LT)	N/A	37.3 (21.5–50.4)	35.0 (16.8–47.2)	31.5 (24.0–38.5)

[a]Values represent the medians for each measurement period. Values in parentheses are the 25th and 75th percentiles.

estimated using the empirical formula given by *Ehhalt and Rohrer* [2000]. The empirical formula includes the NO_2 mixing ratio and photolysis frequencies ($J(NO_2)$ and $J(O^1D)$) as input parameters. The $J(NO_2)$ and $J(O^1D)$ were measured using a filter radiometer [*Kita et al.*, 2002] during the summer, fall, and winter2 period and also measured using a spectroradiometer [*McKenzie et al.*, 2002] during the winter2 period. The filter radiometer data were calibrated by the spectroradiometer data based on their intercomparison during the winter2 period. In situ measurements of OH and HO_2 were made during the winter2 period using a laser-induced fluorescence technique [*Kanaya et al.*, 2001]. We confirmed that the OH concentrations estimated using the empirical formula agreed with the measured OH to within 40% for the winter2 period.

[19] The daytime-averaged OH concentrations ($[OH]_{Day}$) and the daytime-averaged oxidation rates of species X by gas-phase OH reactions (R_X^{Day}) are defined as follows:

$$[OH]_{Day} = \frac{1}{T_{Day}} \int_{Day} [OH] dt \tag{2}$$

$$R_X^{Day} = C_X \frac{1}{T_{Day}} \int_{Day} k_{X+OH}[X][OH] dt, \tag{3}$$

where k_{X+OH} is the rate coefficient of the X + OH reaction, [X] is the number concentration of species X, and C_X is a constant for the unit conversion. The daytime average refers to integration over the time period of 0600–1800 LT (i.e., T_{Day} = 12 hours).

[20] The results for X = NO_2, SO_2, and toluene (C_7H_8) are shown in Table 2. The lifetimes of NO_2, SO_2, and C_7H_8 were calculated using the average values of $[OH]_{Day}$ and temperature during each measurement period. The average and standard deviation of $[OH]_{Day}$ were $(2.2 \pm 1.4) \times 10^6$, $(0.97 \pm 0.48) \times 10^6$, and $(0.78 \pm 0.48) \times 10^6$ cm^{-3} for the summer, fall, and winter2 periods, respectively. The values of R_{NO2}^{Day}, R_{SO2}^{Day}, and R_{C7H8}^{Day} are expressed in the units of μg (as NO_3) m^{-3} hr^{-1}, μg (as SO_4) m^{-3} hr^{-1}, and μg (as C) m^{-3} hr^{-1} respectively, so that these values can be directly compared to the mass concentrations of nitrate, sulfate, and organics.

[21] The average values of R_{NO2}^{Day} indicate that the amount of NO_2 oxidized per hour in a unit volume was comparable to the ambient mass concentration of nitrate, suggesting that in situ oxidation (within an hour) of NO_2 by OH could play an important role in determining the mass concentrations of nitrate observed during the measurement periods. Note that loss of total nitrate due to dry deposition of HNO_3 would be small within an hour [*Morino et al.*, 2006]. The average R_{NO2}^{Day} in the summer period was higher by a factor of 1.9 than the winter2 period. *Morino et al.* [2006] have shown that the median ratio of (particulate) nitrate to total nitrate observed at the surface was 0.18 for the summer period and 0.95 for the winter2 period. By combining these two numbers, the average production rate of nitrate during the winter2 period is estimated to be higher by a factor of 2.8 than the summer period. Although the above estimate ignores the dilution/accumulation effect, it can mostly explain the observed difference in the nitrate concentrations between the summer and winter2 periods.

[22] The interpretation of sulfate can be more complicated than nitrate because of the longer lifetime of SO_2 than NO_2 against OH reactions and the faster deposition velocity of SO_2 than NO_2. In situ oxidation of SO_2 by aqueous phase reactions would be slow in this case because there was no significant amount of liquid water (i.e., cloud/fog droplets) in the observed air masses. Details of the formation and removal of SO_2 and sulfate during the measurement period will be presented elsewhere (T. Miyakawa et al., manuscript in preparation, 2006). The average values of R_{SO2}^{Day} indicate that the amount of SO_2 oxidized per hour in a unit volume was much smaller than the ambient mass concentrations of sulfate, suggesting that in situ oxidation of SO_2 by OH played a minor role in determining the mass concentrations of sulfate observed during the measurement periods. It is likely that the majority of the observed sulfate was produced somewhere upstream of the RCAST observatory either by gas-phase or aqueous-phase reactions. However, we should note that the higher R_{SO2}^{Day} in the summer period is qualitatively consistent with the higher mass concentration of sulfate observed during the summer period.

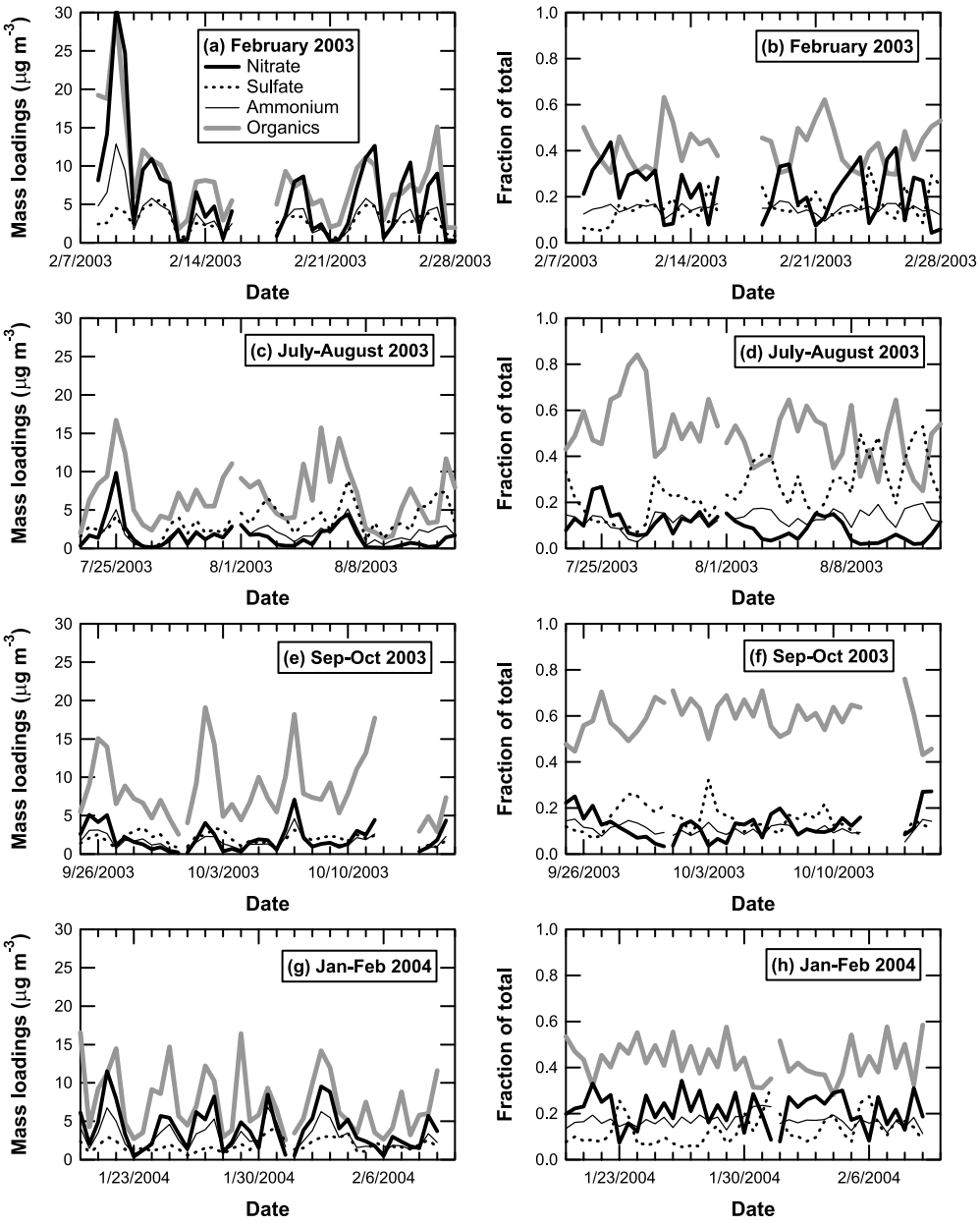

Figure 6. (a) Mass concentrations of nitrate (bold line), sulfate (dashed line), ammonium (thin line), and organics (shaded line) and (b) their fractions of total nonrefractory (NR) PM_1 mass in the winter1 periods. The data are 12 hour averages. (c, d) Same as Figures 6a and 6b, but for the summer period. (e, f) Same as Figures 6a and 6b, but for the fall period. (g, h) Same as Figure 6a and 6b, but for the winter2 period.

Table 2. Lifetime and Oxidation Rate by OH Reaction During Daytime (0600–1800 LT)

	Summer (Jul–Aug 2003)		Fall (Sep–Oct 2003)		Winter2 (Jan–Feb 2004)	
Species	Lifetime,[a] hours	Oxidation rate,[b] μg m^{-3} hr^{-1}	Lifetime,[a] hours	Oxidation rate,[b] μg m^{-3} hr^{-1}	Lifetime,[a] hours	Oxidation rate,[b] μg m^{-3} hr^{-1}
NO_2	14	2.1 ± 0.6	30	1.5 ± 0.5	33	1.1 ± 0.5
SO_2	129	0.09 ± 0.14	283	0.013 ± 0.008	328	0.019 ± 0.013
C_7H_8	22	0.23 ± 0.11	48	0.18 ± 0.09	56	0.14 ± 0.05

[a]The lifetimes of NO_2, SO_2, and C_7H_8 were calculated using the average OH concentrations and temperatures at 0600–1800 LT (daytime) for each measurement period. The OH concentrations were estimated using the empirical formula given by *Ehhalt and Rohrer* [2000]. The average OH concentrations at 0600–1800 LT were 2.2×10^6, 0.97×10^6, and 0.78×10^6 cm^{-3} for the summer, fall, and winter2 periods, respectively.

[b]See text for the definition of the oxidation rates. Values represent the average ±1σ.

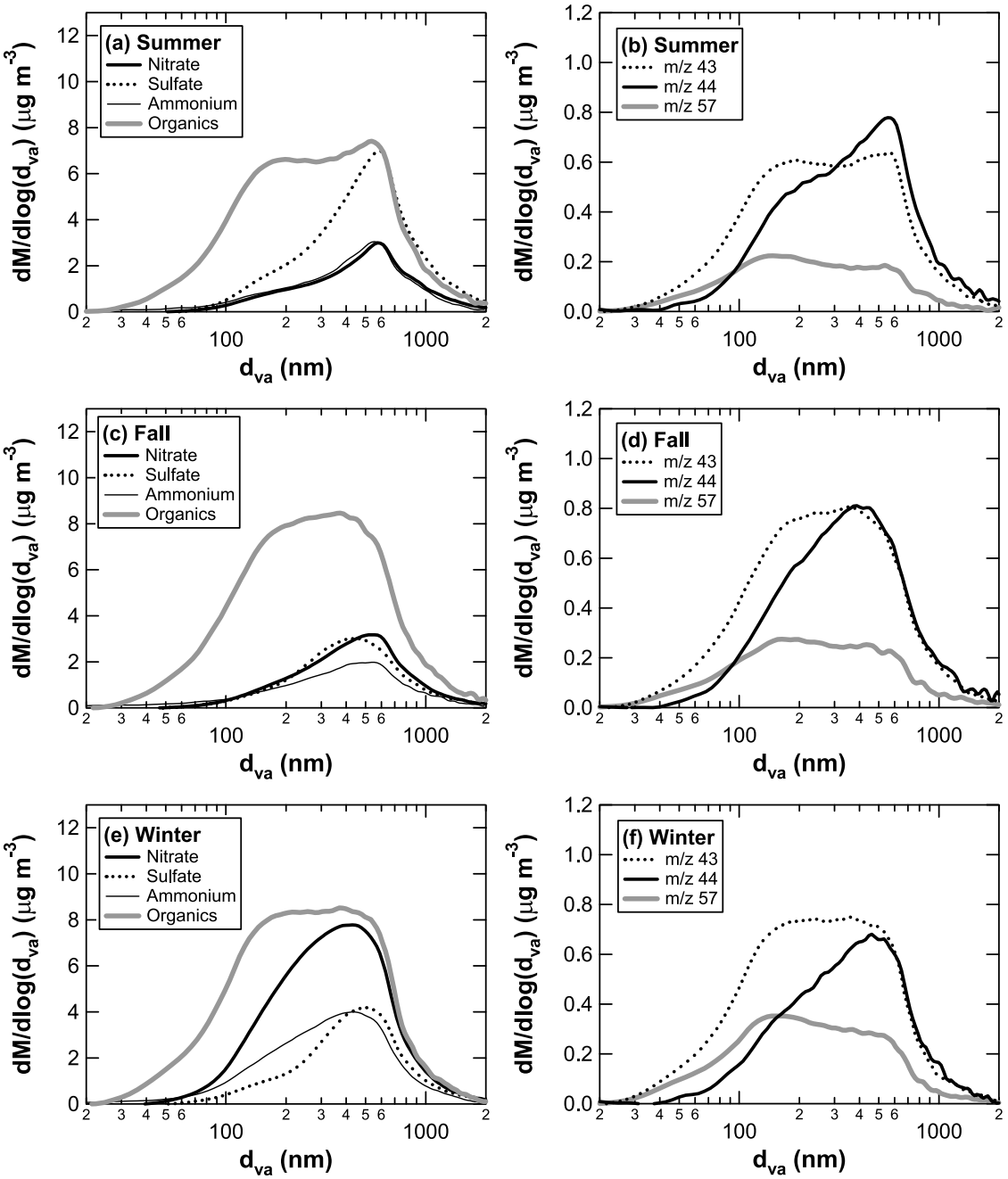

Figure 7. (a) Average size distributions of nitrate (bold line), sulfate (dashed line), ammonium (thin line), and organics (shaded line) in the summer period. The horizontal axis is the vacuum aerodynamic diameter (d_{va}). (b) Average size distributions of m/z 43 (dashed line), m/z 44 (solid line), and m/z 57 (shaded line) in the summer period. (c, d) Same as Figures 7a and 7b, but for the fall period. (e, f) Same as Figures 7a and 7b, but for the winter period.

3.2. Size Distributions

[23] Figures 7a, 7c, and 7e show the average size distributions of nitrate, sulfate, ammonium, and organics in the summer, fall, and winter periods, respectively. The horizontal axis is the vacuum aerodynamic diameter (d_{va}) [*Jimenez et al.*, 2003b; *DeCarlo et al.*, 2004]. The characteristics of the organic size distributions described in this paragraph are commonly found in AMS measurements in urban areas [e.g., *Jimenez et al.*, 2003a; *Allan et al.*, 2003; *Alfarra et al.*, 2004; *Zhang et al.*, 2005b]. Organics exhibited bimodal size distributions in both periods. Size distributions of representative fragments of organics (m/z 43, 44, and 57) are plotted in Figures 7b, 7d, and 7f, respectively. Note that m/z 43 represents the equivalent mass concentration of organic fragment represented by the signal intensity at this peak [*Zhang et al.*, 2005a]. The definition of m/z 43 is applicable to other peaks such as m/z 44 and 57. As discussed in the previous AMS

studies mentioned above, m/z 44 (mostly COO^+) is a good marker of oxygenated organic compounds, and m/z 57 (mostly $C_4H_9^+$) is a marker of aliphatic compounds. The peak at m/z 43 is considered to be a mixture of several fragments such as $C_3H_7^+$ and $C_2H_3O^+$. It can be seen that m/z 43 and 57 were in both small (d_{va} < 200 nm) and accumulation (d_{va} > 200 nm) modes, while m/z 44 was mainly, but not entirely, in the accumulation mode. Sulfate and nitrate were also in the accumulation mode in most cases. Although quadrupole AMS measurements do not allow single-particle analysis, the measured size distributions suggest that oxygenated organics were generally internally mixed with inorganic species in Tokyo. As mentioned above, this feature is commonly found in various locations.

3.3. Interpretation of Organic Aerosol

3.3.1. Marker of Oxygenated Organic Compounds (m/z 44)

[24] *Alfarra* [2004] has summarized the m/z 44/OA ratios of aerosols from various sources/locations based on field measurements and laboratory experiments [*Alfarra et al.*, 2004; *Canagaratna et al.*, 2004; *Topping et al.*, 2004]. The m/z 44/OA ratio increased from <0.01 in the case of unburned diesel fuel and lubricating oil to ~0.19 for Suwannee River fulvic acid. The relevance of using m/z 44 (and m/z 57) as a reliable marker of oxygenated (and hydrocarbon-like) organic aerosol has been further investigated by *Zhang et al.* [2005a].

[25] Figure 8 shows a histogram of m/z 44/OA ratios for the summer, fall, and winter periods, where OA represents the mass concentration of organic aerosol. Overall, the m/z 44/OA ratios in Tokyo ranged from ~0 to 0.19 during the measurement periods. The histogram does not significantly change even though we only use the data strongly influenced by local emissions (i.e., CO mixing ratios larger than the median), suggesting that the observed variability in the m/z 44/OA ratios was not primarily due to mixing of local emissions with aged background air but was mainly due to photochemical processing of local emissions. Although our measurements were made near emission sources in an urban area, the observed m/z 44/OA ratios cover the variability range of the m/z 44/OA ratios given by *Alfarra* [2004]. This result suggests that we observed air masses with a variety of photochemical ages, from fresh primary emissions to highly processed air, and that significant photochemical processing could occur even in urban regions.

[26] We can clearly see a seasonal shift in the histogram during the measurement periods. The modal m/z 44/OA ratios were 0.08–0.09, 0.06–0.07, and 0.05–0.06 for the summer, fall, and winter periods, respectively. As described in section 3.1, the daytime average OH concentration in the summer period was higher by a factor of ~2.8 than the winter2 periods. The seasonal shift in the m/z 44/OA ratios is qualitatively consistent with the seasonal difference in the OH concentrations because faster oxidation of VOCs produces more oxygenated organic compounds and may give rise to more multifunctional species in the SOA. For example, the average oxidation rate of toluene, which is recognized as an important SOA precursor in urban air [*Odum et al.*, 1997], was 0.23 μgC m^{-3} hr^{-1} and 0.14 μgC m^{-3} hr^{-1} for the summer and winter2 periods, respectively (Table 2).

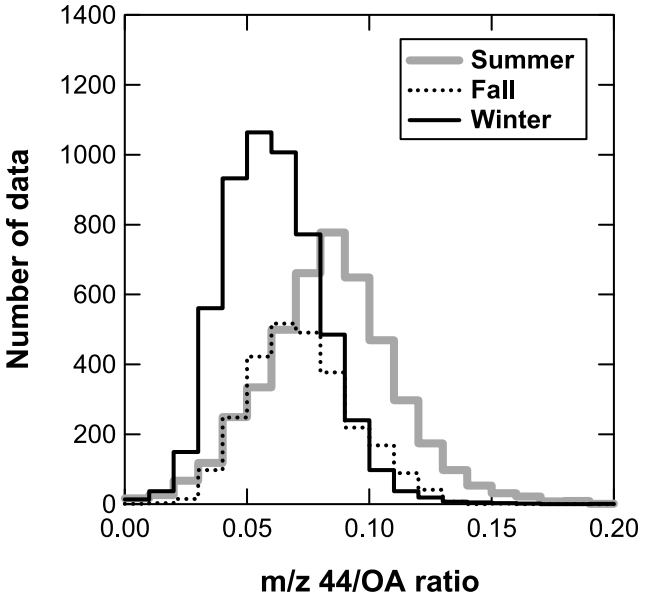

Figure 8. Histogram of m/z 44/OA ratios for the summer (shaded line), fall (dashed line), and winter (solid line) periods.

3.3.2. Classification of Organic Aerosol

[27] The observed mass concentrations of organic aerosol are divided into three groups, which approximately correspond to regional background air, local primary emission, and local secondary formation. First, we define the concentrations of CO and organic aerosols in regional background air (upwind and/or free tropospheric air). The CO mixing ratio in regional background air was defined as an average of the lowest 5% CO mixing ratios for each measurement period (Table 3). The background concentration of OA was determined using the same data points as used to define the background CO mixing ratios. Assuming a constant background level for each measurement period, the enhancement of chemical species X (ΔX) is calculated by subtracting the background level (X_{BG}) from ambient concentration, where X represents CO and OA:

$$\Delta CO = CO - CO_{BG} \quad (4)$$

$$\Delta OA = OA - OA_{BG}. \quad (5)$$

The background levels of CO and OA were slightly higher in the winter period than the summer period. On a regional scale, air masses were transported from the Asian continental region in winter, while they were transported from the western Pacific in summer (section 2.2). This may cause the seasonal difference in the background levels between the winter and summer periods. The ΔOA is further divided into two groups using the correlation with CO. The combustion-related organic aerosol (combustion OA) is defined as the POA fraction that has a linear correlation with ΔCO. The excess organic aerosol (excess

Table 3. Background Concentrations[a]

Species	Winter1 (Feb 2003)	Summer (Jul–Aug 2003)	Fall (Sep–Oct 2003)	Winter2 (Jan–Feb 2004)
CO, ppbv	213 ± 19	142 ± 20	130 ± 26	243 ± 17
Organics, μg m^{-3}	1.7 ± 1.0	1.6 ± 0.7	2.7 ± 1.1	2.3 ± 0.7

[a]Values represent the average ±1σ. The number of CO data points used for the average is 126, 152, 104, and 120 for the winter1, summer, fall, and winter2 periods, respectively.

OA) is defined by subtracting the combustion OA from ΔOA:

$$\text{Combustion OA} = ER(\text{OA/CO}) \times \Delta\text{CO} \quad (6)$$

$$\text{Excess OA} = \Delta\text{OA} - \text{Combustion OA}, \quad (7)$$

where *ER*(OA/CO) represents the average emission ratio of OA to CO from combustion sources in Tokyo. The determination of *ER*(OA/CO) will be discussed later. Because the basic idea of this definition is the same as for the EC tracer method proposed by *Turpin and Huntzicker* [1995], the definition presented here is referred to as the CO tracer method. If the emissions of POA and CO are dominated by combustion sources and the emission ratio of POA to CO can be regarded as nearly constant, the combustion OA and excess OA may be good approximations of POA and SOA, respectively. However, we use the former terminology for the present analysis to make the definition clear. It should be noted that washout by rain could be a significant removal process of organic aerosol. The number of data points with precipitation greater than 0 mm (per 10 min integration time) was 3–8% of the total number of data points for each measurement period. In this analysis, only data with precipitation equal to zero are selected. The data with nonzero precipitation are not used in this analysis because the number of data points is limited.

[28] In order to estimate the *ER*(OA/CO) values, we need to define "less processed air," corresponding to fresh emissions from combustion sources. A simple definition is to select the air masses observed from midnight to early morning. However, this definition is not sufficient because chemical processing could occur even during the nighttime (e.g., oxidation of VOCs by O_3 and/or NO_3), and because some aged OA may carry over from the previous daytime. *Alfarra* [2004] summarized the *m*/*z* 44/OA and *m*/*z* 57/OA ratios observed in various locations/sources and showed that *m*/*z* 44/OA ratios generally anticorrelate with *m*/*z* 57/OA ratios. For example, *m*/*z* 44/OA and *m*/*z* 57/OA ratios in diesel exhaust from on-road vehicles were found to be ~0.03 and ~0.08, respectively, while those observed in rural areas in Canada were ~0.10 and ~0.02, respectively. A ratio of *m*/*z* 44 to *m*/*z* 57 less than 1 has been found for diesel fuel, lubricating oil, and diesel exhaust, as well as traffic-dominated ambient air. On the basis of the findings of *Alfarra* [2004], we define "less processed air" as the air masses that meet the following three criteria: (1) the air masses were observed at 2200–0800 LT (from late evening to early morning); (2) *m*/*z* 44/OA ratio was smaller than 0.05; and (3) *m*/*z* 57/OA ratio was greater than 0.05.

[29] Correlations of OA versus CO for the less processed air and the rest of the data (i.e., processed air) are plotted in Figure 9. It is important to note that the less processed air data points show reasonably tight correlation (r^2 = 0.80–0.97) and correspond to the lower envelope of the correlation for each measurement period. The average *ER*(OA/CO) was defined as the linear regression slope of the OA-CO correlation for the less processed air, forced through the background. The *ER*(OA/CO) values ranged from 0.011 to 0.014 μg m^{-3} $ppbv^{-1}$, as given in the legend of Figure 9. According to the emission inventory developed by *Kannari et al.* [2004], vehicular sources can account for ~70% of the primary organic carbon (POC) emissions in the regions surrounding the RCAST observatory. This is a fraction similar to the CO emissions (~80%, see section 2.2). The average POC/CO emission ratio from vehicular sources was calculated to be 0.0025 gC g^{-1} = 0.0031 μgC m^{-3} $ppbv^{-1}$ in those regions. The *ER*(OA/CO) values were higher by a factor of 3–5 than the POC/CO emission ratio derived from the inventory. The ratios of organic matter (OM) to OC for typical POA compositions (e.g., ~1.2 for *n*-alkane) do not explain the discrepancy. However, we should note that there could be a substantial uncertainty in the estimate of POC emissions even in an urban area [e.g., *Streets et al.*, 2003].

3.3.3. Evaluation

[30] Possible uncertainties in determining the combustion OA and excess OA are now evaluated. The major uncertainty in determining the combustion OA and excess OA comes from the assumption that (1) the background level of OA is constant during each measurement period, (2) *ER*(OA/CO) is equal to the average emission ratio of POA to CO from combustion sources, and (3) *ER*(OA/CO) is constant during each measurement period.

[31] First, we consider the possible uncertainty associated with the assumption of a constant background. The precision of the background determination is estimated to be ~1 μg m^{-3} based on the standard deviations of the OA concentrations in the background air (Table 3). The accuracy of the background determination is difficult to evaluate. The criterion used in this analysis (CO concentration in lowest 5%) may lead to an underestimate of the background level in some cases if highly polluted air masses (i.e., CO mixing ratios significantly exceed the assumed background level) were transported from outside regions. This effect could be important, especially in wintertime, when air masses were transported mostly from Asian continental regions due to the strong influence of the Siberian High. The CO-CO_2 correlation presented in Figure 4 gives some insights into this effect. *Takegawa et al.* [2004] have shown that $\Delta CO/\Delta CO_2$ ratios from China ranged over 28–48 ppbv $ppmv^{-1}$ in winter. In Tokyo, CO and CO_2 exhibited tight correlation (r^2 = 0.92), and the $\Delta CO/\Delta CO_2$ ratio was found to be 10.7 ppbv $ppmv^{-1}$ in winter. Considering the signif-

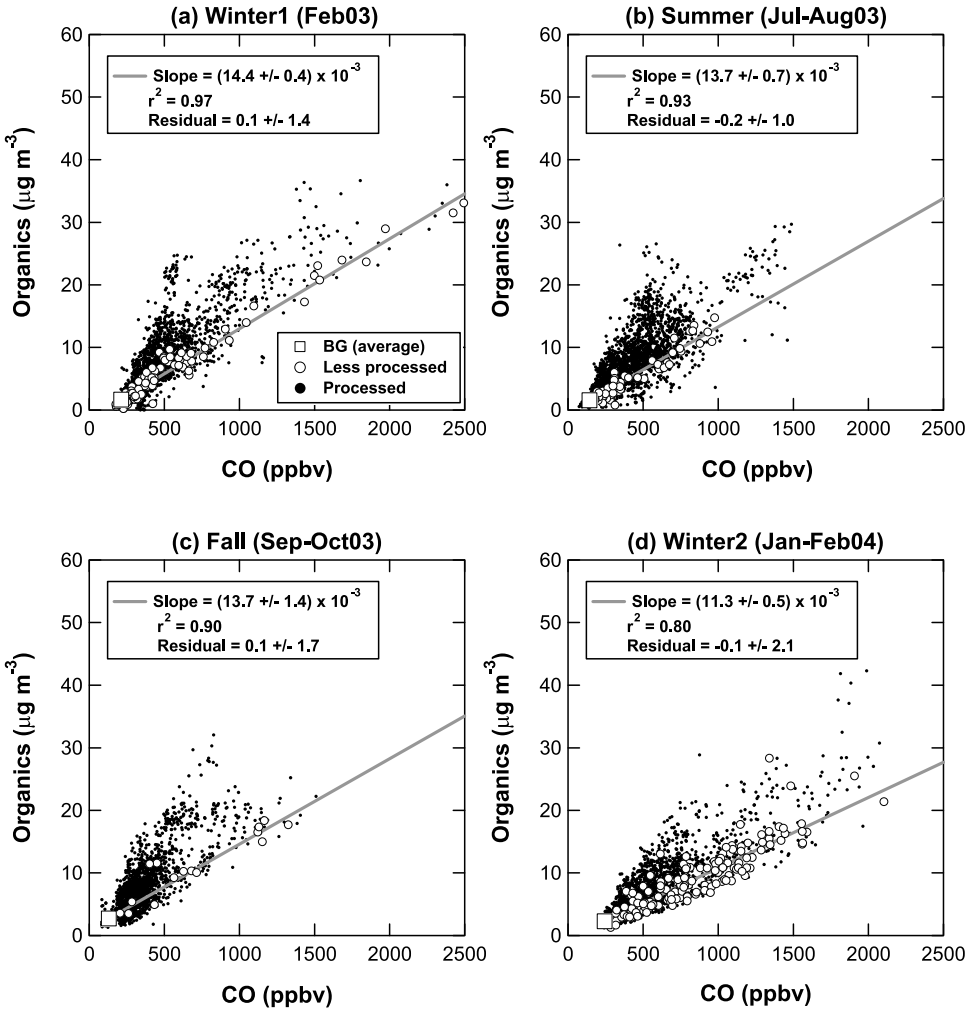

Figure 9. Correlations of OA versus CO in the background air (squares), less processed air (open circles), and processed air (solid circles) for the (a) winter1, (b) summer, (c) fall, and (d) winter2 periods. The background data point represents the average value. The shaded line is the linear regression line for the less processed air (forced through the background). The uncertainty in the slope represents the 95% confidence intervals.

icant difference (by a factor of >2.6) in the $\Delta CO/\Delta CO_2$ ratios between China and Tokyo, it is unlikely that highly polluted air masses transported from Asian continental regions strongly affected the observed concentrations of CO during these periods.

[32] Second, we investigate the possible uncertainty associated with the assumption that *ER*(OA/CO) is equal to the average emission ratio of POA to CO from combustion sources. If there were significant removal and/or oxidation of POA prior to the measurements, *ER*(OA/CO) may not be equal to the emission ratio. The removal of POA due to dry deposition is not taken into account for the present analysis because the dry deposition velocity of fine particles is generally slow [e.g., *Lovett*, 1994]. The oxidation of POA is difficult to evaluate because this process is not well understood. *Robinson et al.* [2006] have recently showed that the photochemical oxidation of some POA compounds can be important on a timescale of a few days. The analysis of HOA during the Pittsburgh Air Quality Study suggested that the oxidation of HOA was not significant on timescales of a few hours [*Zhang et al.*, 2005c]. For the present analysis, the uncertainty due to the oxidation of POA is not taken into account.

[33] Third, the possible uncertainty associated with the assumption of a constant *ER*(OA/CO) is evaluated. The observed correlation of OA with CO for the less processed air is a result of mixing of various plumes from a number of vehicle types (and/or from any other sources). Earlier studies including on-road measurements and chassis dynamometer experiments indicated that the emission factors of organics from vehicular exhaust showed a large variability depending on vehicle type: heavy-duty diesel trucks tend to show higher emission factors than gasoline cars [e.g., *Canagaratna et al.*, 2004; *Rogge et al.*, 1993a]. This tendency is also applicable to the emission factors of EC. *Kondo et al.* [2006] have found that the $\Delta EC/\Delta CO$ ratios (defined as the linear regression slope) observed at RCAST depend significantly on local time and day of

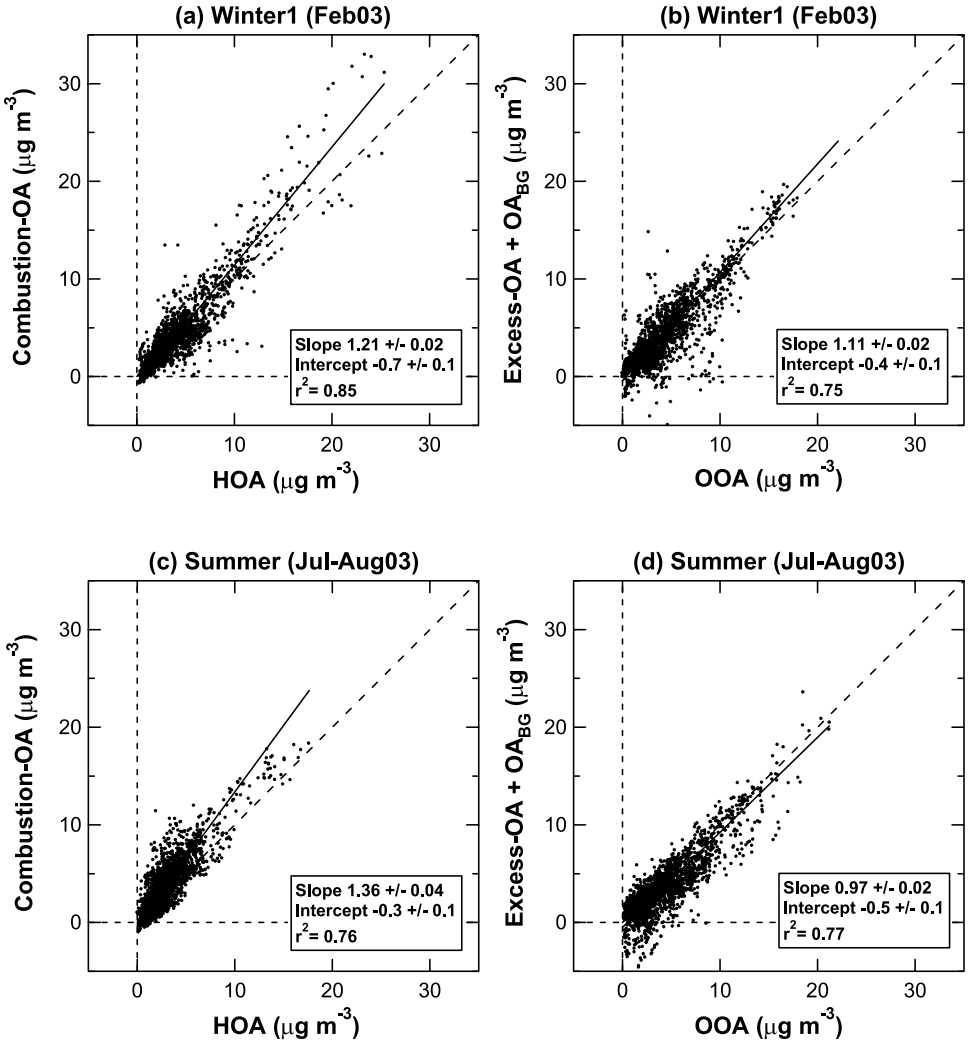

Figure 10. Comparisons of (a) combustion OA versus HOA and (b) excess OA + OA_{BG} versus OOA for the winter1 period. Note that we use a bivariate regression analysis that considers the errors in both variables. (c, d) Same as Figures 10a and 10b, but for the summer period.

week. The $\Delta EC/\Delta CO$ ratios observed in the early morning (0400–0800 LT) were higher by a factor of ~2 than those observed at night (2200–0200 LT), which is consistent with the larger fraction of heavy-duty trucks in the early morning than at night. However, the $\Delta OA/\Delta CO$ ratios in the less processed air did not show such systematic differences corresponding to the fraction of heavy-duty trucks. In addition, the observed $\Delta CO/\Delta CO_2$ ratios did not show significant seasonal and diurnal variations (section 2.2), although the CO/CO_2 emission ratio can also vary depending on the type of vehicles. The most plausible explanation for the observed feature is that the variability in the CO/CO_2 and POA/CO emission ratios from various vehicles was not as large as that in the EC/CO emission ratio. Significant diurnal/decadal variations of EC emission patterns in urban areas have recently been reported by *Harley et al.* [2005]. Therefore it is suggested that the CO tracer method presented in this paper may be better than the traditional EC tracer method in some cases. The additional benefit of using CO as a tracer is that the uncertainty in CO measurements is generally smaller than EC.

[34] The accuracy of the *ER*(OA/CO) is estimated to be ~10%, based on the 95% confidence interval of the linear fit. In order to evaluate the precision of the linear fit, the residual from the linear regression line is defined as

$$\text{Residual} = \Delta OA_{less} - \text{Combustion OA}, \quad (8)$$

where ΔOA_{less} represents the ΔOA values for less processed air. The average ± standard deviation of the residual was found to be 0.1 ± 1.4, −0.2 ± 1.0, 0.1 ± 1.7, and −0.1 ± 2.1 μg m^{-3} for the winter1, summer, fall, and winter2 periods, respectively, and are shown in the legend of Figure 9. The residual did not show significant positive/negative bias. The precision (1σ) of the combustion OA and excess OA is estimated to be ~2 μg m^{-3}, based on the standard deviation of the residual.

[35] Some of the data points categorized as "processed air" show deviations below the *ER*(OA/CO) line (Figure 9),

Table 4. Comparison of Combustion OA/Excess OA versus HOA/OOA

Fit Parameters	Winter1 (Feb 2003)	Summer (Jul–Aug 2003)	Fall (Sep–Oct 2003)	Winter2 (Jan–Feb 2004)
		Combustion OA versus HOA		
Slope[a]	1.21 ± 0.02	1.36 ± 0.04	1.05 ± 0.03	0.88 ± 0.02
Intercept,[a] μg m^{-3}	−0.7 ± 0.1	−0.3 ± 0.1	−0.5 ± 0.1	−0.3 ± 0.1
r^2	0.85	0.76	0.83	0.80
		(Excess OA + OA_{BG}) versus OOA		
Slope[a]	1.11 ± 0.02	0.97 ± 0.02	1.18 ± 0.03	1.41 ± 0.04
Intercept,[a] μg m^{-3}	−0.4 ± 0.1	−0.5 ± 0.1	−0.4 ± 0.1	−1.1 ± 0.2
r^2	0.75	0.77	0.85	0.65

[a]We used a bivariate regression analysis that considers the errors in both variables. Errors represent 2σ.

corresponding to negative concentrations of the excess OA. The root mean square (RMS) values of the negative concentrations were calculated to be 1.4, 1.5, 1.2, and 1.2 μg m^{-3} for the winter1, summer, fall, and winter2 periods, respectively. Although the absolute values of the negative concentrations can be large (> 5 μg m^{-3}) in some cases, the RMS values are found to be within the estimated precision (∼2 μg m^{-3}). This result suggests that the estimated precision is appropriate on average during the measurement periods.

3.3.4. Comparisons of Combustion OA With HOA and Excess OA With OOA

[36] Figure 10 shows the comparisons of combustion OA and HOA and those of excess OA and OOA for the winter1 and summer periods, where HOA and OOA were calculated using the custom principal component analysis [*Zhang et al.*, 2005a]. The sum of excess OA and OA_{BG} is compared with OOA assuming that organic aerosols in the background air were mostly oxygenated (i.e., aged). The regression results for the winter1, summer, fall, and winter2 periods are summarized in Table 4. Here we used a bivariate regression analysis that considers the errors in both variables. We can see tight correlations of combustion OA with HOA (r^2 = 0.76–0.85) and excess OA + OA_{BG} with OOA (r^2 = 0.65–0.85) during the measurement periods. The slope of the combustion OA versus HOA ($S_{ComOA\text{-}HOA}$) ranged from 0.88 to 1.36, while that of the excess OA + OA_{BG} versus OOA ($S_{ExOA\text{-}OOA}$) ranged from 0.97 to 1.41. The sum of $S_{ComOA\text{-}HOA}$ and $S_{ExOA\text{-}OOA}$ for each measurement period ranged from 2.23 to 2.33 (i.e., larger by 12–17% than 2). This is not due to the difference between HOA + OOA and total OA(= combustion OA + excess OA + OA_{BG}) because the regression slope of HOA + OOA versus total OA was ∼0.99 for the winter1, summer, and fall period (∼0.92 for the winter2 period). What we can conclude from these comparisons is that the combustion OA and excess OA agreed with HOA and OOA to within 36% and 41%, respectively, and that there could be uncertainties of 12–17% in those numbers.

3.4. Seasonal and Diurnal Variations of Organic Aerosol

[37] Figures 11a–11b show the time series of CO, O_3, combustion OA, and excess OA observed from 3 to 7 August 2003. The meteorological parameters are plotted in Figures 11c–11d. The Tokyo area was under a stable anticyclone during this period. The weather was mostly sunny (i.e., nonprecipitating), except for rainfall on the afternoon of 5 August 2003. The temperature exceeded 30°C and relative humidity decreased to as low as ∼50% during the daytime. The wind directions were generally southerly during this period, indicating that relatively clean air was transported from the ocean during most of the period. In the morning of 4–6 August 2003, the wind speed was low (∼1 m s^{-1}) and the wind direction drastically changed from north to south. This feature can be interpreted as the turnover of the sea-land breeze circulation and indicates that air masses were stagnant over Tokyo in the morning. The episodes of high O_3 mixing ratios (>80 ppbv) were found on those days. The temporal variation of the excess OA correlated with O_3 during the daytime, showing a maximum of >10 μg m^{-3} at 1200–1400 LT. The ratio of the excess OA to total OA was 0.64–0.84 at those daytime peaks.

[38] Figure 12 shows the diurnal variations of total OA, OA_{BG}, combustion OA, and excess OA in the summer, fall, and winter periods. Average values were calculated in 2 hour bins throughout the day. Although OA_{BG} has a minor contribution to total OA when we consider large enhancements of OA (>10 μg m^{-3}), it becomes important when we consider the average values. While the combustion OA did not exhibit a distinct diurnal variation, there was a clear diurnal pattern for the excess OA (peak at ∼1300 LT), especially in the summer period. At the daytime peak, the excess OA was nearly in the same concentration as the combustion OA for all seasons: the ratio of the average combustion OA to excess OA was 1.3, 1.1, and 1.0 at 1300 LT for the summer, fall, and winter periods, respectively. This result suggests that significant SOA formation occurred during the daytime throughout the measurement periods. The excess OA concentrations were nearly zero at 0100–0700 LT in the summer and winter periods. This feature does not imply that all SOA species disappeared during this time period, because we subtracted the background level from the total OA to define the combustion OA and excess OA. Instead, this can be interpreted as the absence of significant local production of SOA during this time period.

[39] It is interesting to note that a second peak in the excess OA was found at ∼2100 LT. The second peak was even higher than the daytime peak for the winter period. It should be noted that nighttime peaks in SOA were also identified in Atlanta in summer (August 1999) during the Atlanta Supersite Experiment [*Lim and Turpin*, 2002]. There are two possible explanations for the nighttime peaks in the excess OA. The first possibility is that significant

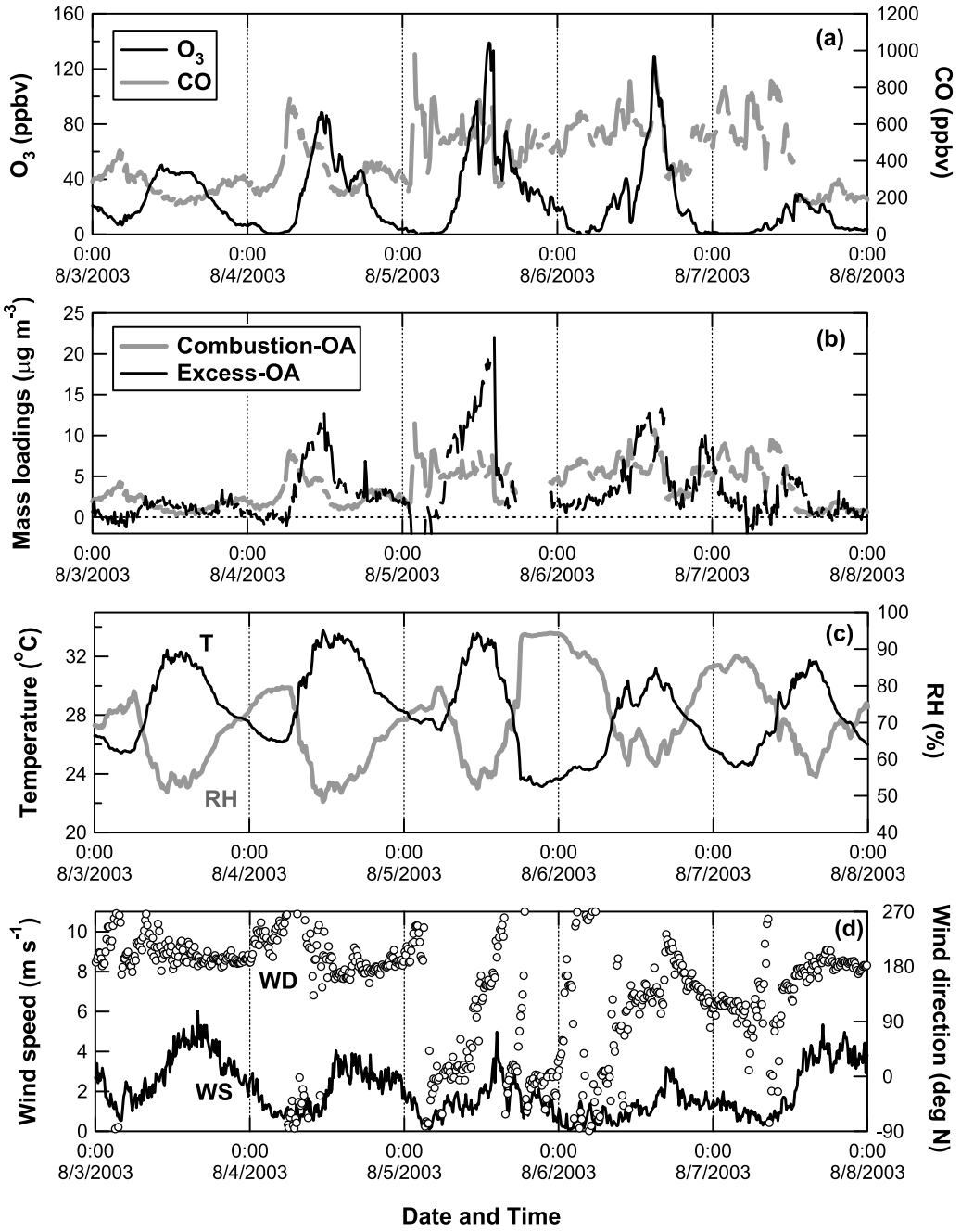

Figure 11. Time series of (a) O_3 (solid line) and CO (shaded line), (b) combustion OA (shaded line) and excess OA (solid line), (c) temperature (solid line) and relative humidity (shaded line), and (d) wind speed (solid line) and wind direction (open circles) observed on 3–7 August 2003.

SOA formation took place even after sunset via reactions of VOCs with O_3 and NO_3. A decrease in the boundary layer height after sunset may have caused additional increase in SOA precursors and/or SOA species formed near the surface. In fact, the combustion OA also showed an increase after sunset. The increase in the combustion OA was evident during the winter period: the median concentration of the combustion OA at 2100 LT was 1.5 times higher than that at 1700 LT. The second possibility is that gas/particle partitioning of condensable organic compounds (COCs) that had been formed during the daytime was shifted toward the particle phase as the temperature decreased after sunset. The gas/particle partitioning of COC species i is given by [*Odum et al.*, 1996]

$$K_{\mathrm{om},i} M_{\mathrm{om}} = A_i / G_i, \tag{9}$$

where $K_{\mathrm{om},i}$ is the gas/particle partitioning constant, M_{om} is the mass concentration of total organic matter in aerosol, A_i is the COC concentration in the aerosol phase, and G_i is the COC concentration in the gas phase. The temperature dependence of COCs formed from photooxidation of aromatics was investigated based on a smog chamber experiment [*Takekawa et al.*, 2003]. Here we estimate the

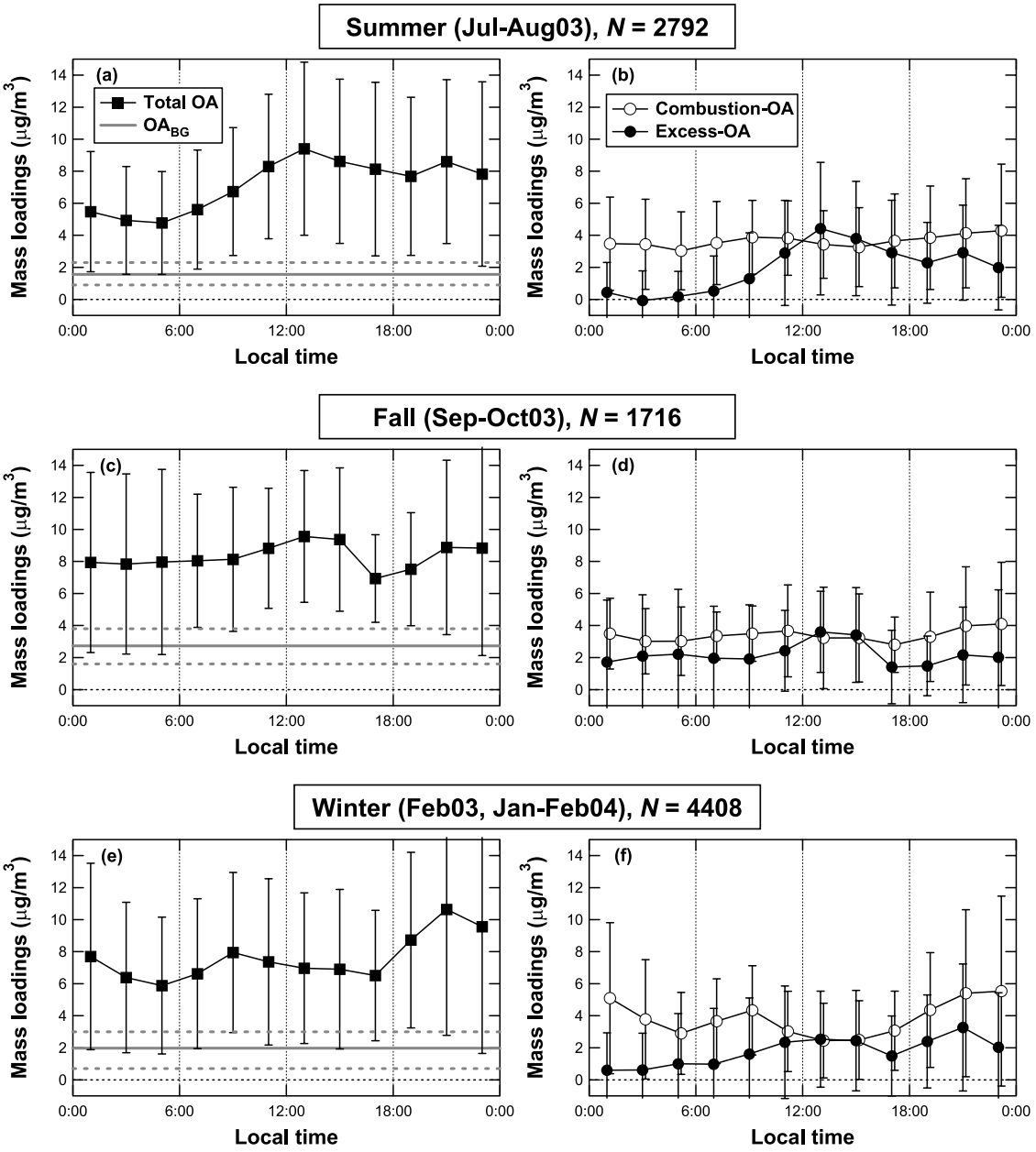

Figure 12. Diurnal variations of (a) total OA (solid squares) and OA_{BG} (shaded line) and (b) combustion OA (open circles) and excess OA (solid circles) in the summer period. Average values were calculated in 2 hour bins throughout the day. Bars indicate the standard deviation. Shaded dashed lines indicate the range of the uncertainty (1σ) in OA_{BG}. The number of data points (N) is also indicated. (c, d) Same as Figures 12a and 12b, but for the fall period. (e, f) Same as Figures 12a and 12b, but for the winter period.

effect of temperature on gas/particle partitioning of COCs formed from toluene during the winter period, based on the results of *Takekawa et al.* [2003]. Assuming a constant M_{om} of 6 μg m^{-3} (median in the winter period), the A_i/G_i ratio at 2100 LT (279K) is estimated to be 14% higher than that at 1300 LT (282 K). COCs formed from other aromatics such as *m*-xylene and 1,2,4-trimethylbenzene showed a stronger temperature dependence than toluene [*Takekawa et al.*, 2003]. Therefore the nighttime peak during the winter period may be partially due to the shift in the gas/particle equilibrium after sunset. A strong dependence of the formation rate and gas/particle partitioning of COCs on temperature has previously been discussed by *Strader et al.* [1999], based on the data set obtained in the San Joaquin Valley of California during the winter of 1995–1996.

4. Summary and Conclusions

[40] We have conducted ground-based measurements of NR-PM_1 aerosol in Tokyo using the AMS from February 2003 to February 2004. Organic compounds were found to be the dominant component throughout the measurement

periods (40–60% of the total NR-PM_1 mass). The ratio of m/z 44 (marker of oxygenated organic compounds) to OA showed a clear seasonal shift (higher in summer), which was qualitatively consistent with the higher OH concentrations in summer than winter.

[41] The mass concentrations of OA were divided into three groups (background OA, combustion OA, and excess OA) based on the correlation with CO. It was found that the combustion OA and excess OA + OA_{BG} were similar to HOA and OOA, respectively, during the measurement periods. On average, the excess OA showed a clear diurnal pattern (daytime peak at ~1300 LT), especially in the summer period. At the daytime peak, the average concentration of the excess OA was nearly equal to that of the combustion OA for all periods, suggesting that significant SOA formation occurred in daytime throughout the measurement period. A second peak in the excess OA was found at ~2100 LT, especially in the winter period. This may be due to a formation of SOA via reactions of VOCs with O_3 and NO_3 after sunset, and/or to a shift in the gas/particle equilibrium of SOA compounds after sunset.

[42] **Acknowledgments.** The authors thank J. D. Allan for providing the AMS analysis software. We appreciate Y. Yokouchi for providing the VOC data, and we also appreciate R. McKenzie, P. Johnston, and K. Kita for providing the $J(O^1D)$ and $J(NO_2)$ data. The routine monitoring data were obtained by the Tokyo Metropolitan Government. This study was funded by the Japanese Ministry of Education, Culture, Sports, Science and Technology (MEXT) and the Japanese Science and Technology Agency (JST). The participation in this work of J.L.J. and Q.Z. has been supported by NSF grant ATM-0449815 and EPA grant RD-83216101-0.

References

Alfarra, M. R. (2004), Insights into atmospheric organic aerosols using an aerosol mass spectrometer, Ph.D. thesis, University of Manchester, U. K.

Alfarra, M. R., et al. (2004), Characteristics of urban and rural organic particulate in the Lower Fraser Valley using two Aerodyne aerosol mass spectrometers, *Atmos. Environ.*, *38*, 5745–5758.

Allan, J. D., et al. (2003), Quantitative sampling using an Aerodyne aerosol mass spectrometer: 2. Measurements of fine particulate chemical composition in two U.K. cities, *J. Geophys. Res.*, *108*(D3), 4091, doi:10.1029/2002JD002359.

Alves, C., A. Carvalho, and C. Pio (2002), Mass balance of organic carbon fractions in atmospheric aerosols, *J. Geophys. Res.*, *107*(D21), 8345, doi:10.1029/2001JD000616.

Canagaratna, M. R., et al. (2004), Chase studies of particulate emissions from in-use New York City vehicles, *Aerosol Sci. Technol.*, *38*, 555–573.

Chow, J. C., J. W. Watson, E. M. Fujita, Z. Lu, D. R. Lawson, and L. L. Ashbaugh (1994), Temporal and spatial variations of PM2.5 and PM10 aerosol in the Southern California Air Quality Study, *Atmos. Environ.*, *28*, 2061–2080.

DeCarlo, P., J. G. Slowik, D. R. Worsnop, P. Davidovits, and J. L. Jimenez (2004), Particle morphology and density characterization by combined mobility and aerodynamic diameter measurements. part 1: Theory, *Aerosol Sci. Technol.*, *38*, 1185–1205.

Ehhalt, D. H., and F. Rohrer (2000), Dependence of the OH concentration on solar UV, *J. Geophys. Res.*, *105*, 3565–3571.

Enomoto, T., Y. Yokouchi, K. Izumi, and T. Inagaki (2005), Development of an analytical method for atmospheric halocarbons and its application to airborne observation (in Japanese), *J. Jpn. Soc. Atmos. Environ.*, *40*, 1–8.

Gray, H. A., G. R. Cass, J. J. Huntzicker, E. K. Heyerdahl, and J. A. Rau (1986), Characteristics of atmospheric organic and elemental carbon particle concentrations in Los Angeles, *Environ. Sci. Technol.*, *20*, 580–582.

Harley, R. A., L. C. Marr, J. K. Lehner, and S. N. Giddings (2005), Changes in motor vehicle emissions on diurnal to decadal time scales and effects on atmospheric composition, *Environ. Sci. Technol.*, *39*, 5356–5362.

Jayne, J. T., D. C. Leard, X. F. Zhang, P. Davidovits, K. A. Smith, C. E. Kolb, and D. R. Worsnop (2000), Development of an aerosol mass spectrometer for size and composition analysis of submicron particles, *Aerosol Sci. Technol.*, *33*, 49–70.

Jimenez, J. L., et al. (2003a), Ambient aerosol sampling using the Aerodyne aerosol mass spectrometer, *J. Geophys. Res.*, *108*(D7), 8425, doi:10.1029/2001JD001213.

Jimenez, J. L., R. Bahreini, D. R. Cocker III, H. Zhuang, V. Varutbangkul, R. C. Flagan, J. H. Seinfeld, C. D. O'Dowd, and T. Hoffmann (2003b), New particle formation from photooxidation of diiodomethane (CH_2I_2), *J. Geophys. Res.*, *108*(D10), 4318, doi:10.1029/2002JD002452.

Kajino, M., H. Ueda, H. Satsumabayashi, and Z. Han (2005), Increase in nitrate and chloride deposition in east Asia due to increased sulfate associated with the eruption of Miyakejima Volcano, *J. Geophys. Res.*, *110*, D18203, doi:10.1029/2005JD005879.

Kanaya, Y., Y. Sadanaga, J. Hirokawa, Y. Kajii, and H. Akimoto (2001), Development of a ground-based LIF instrument for measuring tropospheric HO_x radicals: Instrumentation and calibrations, *J. Atmos. Chem.*, *38*, 73–110.

Kannari, A., T. Baba, H. Ueda, Y. Tonooka, and K. Matsuda (2004), Development of a grid database on atmospheric pollutants emissions in Japan (in Japanese), *J. Jpn. Soc. Atmos. Environ.*, *39*, 257–271.

Kawamura, K., and K. Ikushima (1993), Seasonal changes in the distribution of dicarboxylic acids in the urban atmosphere, *Environ. Sci. Technol.*, *27*, 2227–2235.

Kawamura, K., and I. R. Kaplan (1987), Motor exhaust emissions as a primary source for dicarboxylic acids in Los Angeles ambient air, *Environ. Sci. Technol.*, *21*, 105–110.

Kita, K., et al. (2002), Photochemical production of ozone in the upper troposphere in association with cumulus convection over Indonesia, *J. Geophys. Res.*, *108*(D3), 8400, doi:10.1029/2001JD000844.

Kondo, Y., S. Kawakami, M. Koike, D. W. Fahey, H. Nakajima, Y. Zhao, N. Toriyama, M. Kanada, G. W. Sachse, and G. L. Gregory (1997), Performance of an aircraft instrument for the measurement of NO_y, *J. Geophys. Res.*, *102*, 28,663–28,671.

Kondo, Y., et al. (2006), Temporal variations of elemental carbon in Tokyo, *J. Geophys. Res.*, doi:10.1029/2005JD006257, in press.

Lim, H.-J., and B. J. Turpin (2002), Origins of primary and secondary aerosol in Atlanta: Results of time-resolved measurements during the Atlanta Supersite Experiment, *Environ. Sci. Technol.*, *36*, 4489–4496.

Lovett, G. M. (1994), Atmospheric deposition of nutrients and pollutants in North America: An ecological perspective, *Ecol. Appl.*, *4*, 629–650.

McKenzie, R., P. Johnston, A. Hofzumahaus, A. Kraus, S. Madronich, C. Cantrell, J. Calvert, and R. Shetter (2002), Relationship between photolysis frequencies derived from spectroscopic measurements of actinic fluxes and irradiances during the IPMMI campaign, *J. Geophys. Res.*, *107*(D5), 4042, doi:10.1029/2001JD000601.

Morino, Y., Y. Kondo, N. Takegawa, Y. Miyazaki, K. Kita, Y. Komazaki, M. Fukuda, T. Miyakawa, N. Moteki, and D. R. Worsnop (2006), Partitioning of HNO_3 and particulate nitrate over Tokyo: Effect of vertical mixing, *J. Geophys. Res.*, doi:10.1029/2005JD006887, in press..

NARSTO (2004), *Particulate Matter Assessment for Policy Makers: A NARSTO Assessment*, edited by P. McMurry, M. Shepherd, and J. Vickery, Cambridge Univ. Press, New York.

Odum, J. R., T. Hoffmann, F. Bowman, D. Collins, R. C. Flagan, and J. H. Seinfeld (1996), Gas/particle partitioning and secondary organic aerosol yields, *Environ. Sci. Technol.*, *30*, 2580–2585.

Odum, J. R., T. P. W. Jungkamp, R. J. Griffin, R. C. Flagan, and J. H. Seinfeld (1997), The atmospheric aerosol-forming potential of whole gasoline vapor, *Science*, *276*, 96–99.

Reilly, P. T. A., R. A. Gieray, W. B. Whitten, and J. M. Ramsey (1998), Real-time characterization of the organic composition and size of individual diesel engine smoke particles, *Environ. Sci. Technol.*, *32*, 2672–2679.

Robinson, A. L., N. M. Donahue, and W. F. Rogge (2006), Photochemical oxidation and changes in molecular composition of organic aerosol in the regional context, *J. Geophys. Res.*, *111*, D03302, doi:10.1029/2005JD006265.

Rogge, W. F., L. M. Hildemann, M. A. Mauzrek, G. R. Cass, and B. R. T. Simoneit (1993a), Sources of fine organic aerosol. 2. Noncatalyst and catalyst-equipped automobiles and heavy-duty diesel trucks, *Environ. Sci. Technol.*, *27*, 636–651.

Rogge, W. F., M. A. Mazurek, L. M. Hildemann, G. R. Cass, and B. R. T. Simoneit (1993b), Quantification of urban organic aerosols at a molecular level: Identification, abundance and seasonal variation, *Atmos. Environ.*, *27*, 1309–1330.

Saxena, P., and L. M. Hildemann (1996), Water-soluble organics in atmospheric particles: A critical review of the literature and application of thermodynamics to identify candidate compounds, *J. Atmos. Chem.*, *24*, 57–109.

Saxena, P., L. M. Hildemann, P. H. McMurry, and J. H. Seinfeld (1995), Organics alter hygroscopic behavior of atmospheric particles, *J. Geophys. Res.*, *100*, 18,755–18,770.

Strader, R., F. Lurmann, and S. N. Pandis (1999), Evaluation of secondary aerosol formation in winter, *Atmos. Environ.*, *33*, 4849–4863.

Streets, D. G., et al. (2003), An inventory of gaseous and primary aerosol emissions in Asia in the year 2000, *J. Geophys. Res.*, *108*(D21), 8809, doi:10.1029/2002JD003093.

Sullivan, A. P., R. J. Weber, A. L. Clements, J. R. Turner, M. S. Bae, and J. J. Schauer (2004), A method for on-line measurement of water-soluble organic carbon in ambient aerosol particles: Results from an urban site, *Geophys. Res. Lett.*, *31*, L13105, doi:10.1029/2004GL019681.

Szidat, S., et al. (2004), Radiocarbon (C-14)-deduced biogenic and anthropogenic contributions to organic carbon (OC) of urban aerosols from Zurich, Switzerland, *Atmos. Environ.*, *38*, 4035–4044.

Takekawa, H., H. Minoura, and S. Yamazaki (2003), Temperature dependence of secondary organic aerosol formation by photo-oxidation of hydrocarbons, *Atmos. Environ.*, *37*, 3413–3424.

Takegawa, N., et al. (2004), Removal of NO_x and NO_y in Asian outflow plumes: Aircraft measurements over the western Pacific in January 2002, *J. Geophys. Res.*, *109*, D23S04, doi:10.1029/2004JD004866.

Takegawa, N., Y. Miyazaki, Y. Kondo, Y. Komazaki, T. Miyakawa, J. L. Jimenez, J. T. Jayne, D. R. Worsnop, J. Allan, and R. J. Weber (2005), Characterization of an Aerodyne aerosol mass spectrometer (AMS): Intercomparison with other aerosol instruments, *Aerosol Sci. Technol.*, *39*, 760–770.

Tobias, H. J., D. E. Beving, P. J. Ziemann, H. Sakurai, M. Zuk, P. H. McMurry, D. Zarling, R. Waytulonis, and D. B. Kittelson (2001), Chemical analysis of diesel engine nanoparticles using a nano-DMA/thermal desorption particle beam mass spectrometer, *Environ. Sci. Technol.*, *35*, 2233–2243.

Topping, D., H. Coe, G. McFiggans, R. Burgess, J. Allan, M. R. Alfarra, K. Bower, T. W. Choularton, S. Decesari, and M. C. Facchini (2004), Aerosol chemical characteristics from sampling conducted on the Island of Jeju, Korea during ACE-Asia, *Atmos. Environ.*, *38*, 2111–2123.

Turpin, B. J., and J. J. Huntzicker (1995), Identification of secondary organic aerosol episodes and quantitation of primary and secondary organic aerosol concentrations during SCAQS, *Atmos. Environ.*, *29*, 3527–3544.

Turpin, B. J., P. Saxena, and E. Andrews (2000), Measuring and simulating particulate organics in the atmosphere: Problems and prospects, *Atmos. Environ.*, *34*, 2983–3013.

Zhang, Q., M. R. Alfarra, D. R. Worsnop, J. D. Allan, H. Coe, M. R. Canagaratna, and J. L. Jimenez (2005a), Deconvolution and quantification of hydrocarbon-like and oxygenated organic aerosols based on Aerosol Mass Spectrometry, *Environ. Sci. Technol.*, *39*, 4938–4952.

Zhang, Q., M. R. Canagaratna, J. T. Jayne, D. R. Worsnop, and J.-L. Jimenez (2005b), Time- and size-resolved chemical composition of submicron particles in Pittsburgh: Implications for aerosol sources and processes, *J. Geophys. Res.*, *110*, D07S09, doi:10.1029/2004JD004649.

Zhang, Q., D. R. Worsnop, M. R. Canagaratna, and J. L. Jimenez (2005c), Hydrocarbon-like and oxygenated organic aerosols in Pittsburgh: Insights into sources and processes of organic aerosols, *Atmos. Chem. Phys.*, *5*, 3289–3311.

M. Fukuda, Y. Kondo, T. Miyakawa, and N. Takegawa, Research Center for Advanced Science and Technology, University of Tokyo, 4-6-1 Komaba, Meguro, Tokyo 153-8904, Japan. (takegawa@atmos.rcast.u-tokyo.ac.jp)

J. L. Jimenez, Department of Chemistry and Biochemistry, University of Colorado, Boulder, CO 80309, USA.

D. R. Worsnop, Center for Aerosol and Cloud Chemistry, Aerodyne Research, Inc., 45 Manning Road, Billerica, MA 01821, USA.

Q. Zhang, Atmospheric Science Research Center, University at Albany, State University of New York, 251 Fuller Road, Albany, NY 12203, USA.